ELSEVIER

Biophysical Chemistry 76 (1999) 35–53

Biophysical Chemistry

Molecular dynamics simulations of the ErbB-2 transmembrane domain within an explicit membrane environment: comparison with vacuum simulations

Jean-Pierre Duneau[a], Serge Crouzy[b], Norbert Garnier[a], Yves Chapron[b], Monique Genest[a,*]

[a] *Centre de Biophysique Moléculaire, CNRS, Rue Charles Sadron, 45071 Orléans Cedex 02, France*
[b] *Département de Biologie Moléculaire et Structurale, Laboratoire de Biophysique Moléculaire et Cellulaire, CENG, CEA, 17 Rue des Martyrs, 38054 Grenoble Cedex 9, France*

Received 27 May 1998; received in revised form 2 November 1998; accepted 2 November 1998

Abstract

Two 500-ps molecular dynamics simulations performed on the single transmembrane domain of the ErbB-2 tyrosine kinase receptor immersed in a fully solvated dilauroylphosphatidyl-ethanolamine bilayer (DLPE) are compared to vacuum simulations. One membrane simulation shows that the initial α helix undergoes a local π helix conversion in the peptide part embedded in the membrane core similar to that found in simulation vacuum. Lipid/water/peptide interaction analysis shows that in the helix core, the intramolecular peptide interactions are largely dominant compared to the interactions with water and lipids whereas the helix extremities are much more sensitive to these interactions at the membrane interfaces. Our results suggest that simulations in a lipid environment are required to understand the dynamics of transmembrane helices, but can be reasonably supplemented by in vacuo simulations to explore rapidly its conformational space and to describe the internal deformation of the hydrophobic core.

Keywords: Receptor protein-tyrosine kinase; Structure–dynamics activity relationships; α Helix stability; $\alpha \rightarrow \pi$ Helix transition; Membrane environment

1. Introduction

Molecular dynamics (MD) simulation is a useful tool for describing at atomic resolution the motions affecting protein structures [1]. It has been successful in reproducing experimental observations in a growing number of cases [2–4], it is now becoming routinely used to monitor structural transitions and dynamics on a nanosecond time scale. Such an improvement in the reliability of molecular dynamics simulations comes mostly from the explicit account of water

* Corresponding author. Tel.: +33 2 38257668; fax: +33 2 38631517; e-mail: geneste@cnrs-orleans.fr

0301-4622/99/$ - see front matter
PII:S0301-4622(98)00216-6

molecules in a soluble protein environment [5]. Water is an integral component of the protein structure by its ability to form hydrogen bonds and to modify the accessible conformational space around the average X-ray or NMR structure [6–8].

Through entropy, water is also responsible for hydrophobic effects allowing the correct folding of the proteins and therefore their functions [9–12]. Although there is some promising way to implicitly model hydration effects [13], considering explicitly an aqueous environment is nowadays a standard in spite of the considerable increase of computational resources it requires. However, long time scales are not easily accessible and the study of the reproducibility of the observed phenomenon is difficult.

In the case of intrinsic membrane proteins the natural environment is mostly anhydrous. Membrane proteins are composed of regions exposed to the solvent distinct to regions embedded in the membrane. The extramembrane parts contain a significant amount of hydrophilic residues and roughly behave as soluble proteins whereas the intramembrane part, composed mostly of hydrophobic residues constituting the transmembrane domains (TM) is not affected by water molecules [14]. Polar groups of the main chain are buried and are involved in intra-molecular hydrogen bonds restricting their structure to mainly helices or sheets with none or few disrupted hydrogen bonds [15].

The membrane environment effect is experimentally evidenced when structureless soluble peptides become structured when they are embedded in membrane vesicles, bilayers or monolayers [16–19]. The same structuring effect is also observed in apolar solvents which stabilize secondary structures [20]. A similar behavior is observed when performing a molecular dynamics (MD) simulation in a vacuum of polyalanine which is maintained in a stable helix structure while it unfolds in a few picoseconds in a water environment [21].

The structuring effect of the apolar medium justifies theoretical works devoted to study the structure and the dynamics of TM domains without explicit lipid environment considering a low dielectric constant as a reasonable approximation [22–25]. The complexity of membrane simulations may also justify the use of a vacuum although nowadays, they are becoming very accurate in reproducing many experimental data [26,27] as a result of increasing computer power and force field improvement [28]. Therefore, the possibility arises now of examining the effect of an explicit lipid environment on the behavior of inserted transmembrane peptides but on a limited time scale.

Nevertheless, if some properties of membrane proteins could be predicted in vacuum. studies of the dynamics of single transmembrane domains and their association in complexes could be performed easily on a large time scale. It is thus of great interest to compare the results of MD simulations of helical structures performed in vacuum and in an explicit lipid environment and this is the aim of the present study.

Our laboratory has been involved in the understanding of transduction signal mechanisms for a few years, and particularly of the role of the single TM of tyrosine kinase receptors of the ErbB-2 family [29,30]. The deregulation of this protein is involved in many human cancers [31], and it has been shown that a highly specific mutation occurs in the single transmembrane domain at the Val659 site of the whole protein. The mutation that replaces Val659 by Glu constitutively activates the receptor by triggering its dimerization. The ErbB-2 TM has been successfully tested to be a specific target for the transmembrane domain of the deregulated receptor [32] and is expected to be used as a therapeutic agent.

Experimental studies have shown that the ErbB-2 TM is highly helical in a bilayer environment [33]. Moreover, we have demonstrated from 20-ns in vacuo simulations that the helical structure is retained [34] but reproducible conformational transitions affect the helix. These transitions are characterized by the local replacement of the α helix hydrogen bonds (HB) (COi NH i + 4) by a HB pattern characteristic of π helix (COi NH i + 5 HB) according to a well defined mechanism [35]. These transitions do not depend upon simulation parameters but appear strongly related to β-branched residues (Val, Ile, Thr)

largely present in the sequence and also to Gly residues. However, it is important to evaluate the lipid environment effect on the structure and the dynamics of the ErbB-2 TM helix and the fundamental question raised is that of the possibility of such a structural deformation within an explicit membrane bilayer.

To address this point, two distinct 500-ps simulations have been performed on the whole transmembrane domain of the wild receptor embedded in 52 dilauroylphosphatidylethanolamine (DLPE) molecules fully hydrated by 1036 water molecules. The trajectories have been analyzed in terms of HB time series and time autocorrelation functions to investigate the peptide structure and the dynamics of the backbone and the side chains. The peptide behavior within a bilayer model has been compared to that observed in vacuum from multiple 1-ns simulations previously performed [34].

It is important to note that the present study aims at describing the structure and the dynamics of the embedded peptide and not the lipid dynamics. The properties that we have examined prove that our DLPE bilayer model contains at least some structural characteristics of pure lipid membrane that should be sufficient to correctly represent a realistic lipid environment around the transmembrane peptide.

2. Methods

2.1. Peptide

The transmembrane domain extends from residue Leu651 to residue Gln679 of the whole ErbB-2 receptor and includes the hydrophobic core and the presumed juxtamembrane residues inserted at the membrane interfaces. The corresponding sequence of the peptide numbered from 1 to 29 in our model is L_1*T*S*II*SA*VV*$_9$G*I*LL*VV*-*V*LG*VV*FG*I*L*I*KRRQ$_{29}$ with V_9 indicating the site sensitive to the activating E_9 mutation. The *β*-branched residues are shown in italics. The peptide is completed by additional acetyl and *N*-methyl blocking groups at the N- and C-termini, respectively to ensure null charges. The initial structure was built with the SYBYL package [36] in the canonical *α* helix configuration with the standard $\phi = -57°$ and $\varphi = -47°$ dihedral angle values. The χ_1 side chain rotamers of the SYBYL library correspond to those of the backbone-independent rotamer library [37]. In our previous 'in vacuum' study, we reported that the initial side chain conformation does not influence the peptide dynamics and this will not be repeated here.

2.2. Membrane model

The lipid monomer is an L-*α*-dilauroylphosphatidylethanolamine (DLPE) molecule. This lipid was built as a template with the hydrocarbon tails all in a *trans* configuration as observed in the crystal structure [38]. A copy of the initial template was obtained by a 180° rotation followed by a translation to yield the elementary brick of the bilayer. The distance between the two P atoms of the brick was initially 34 Å and the tails interdigitated by approximately four carbon atoms. Twenty-six of these bricks were assembled with all P atoms of each monolayer in the same *YZ* plane to form a cylinder of two concentric rings. The inner ring was composed of 10 lipids separated by 6.64 Å and the outer ring was composed of 16 lipids separated by 6.73 Å (distance P–P). This gave rise to an area per lipid estimated at approximately 50.6 Å^2 and 41 Å^2 for each monolayer, the lower value being obtained for the monolayer in which long side chains of the C-terminal residues of the peptide are embedded. These values are in the same range as experimentally determined for pure L*β* and L*α* phases of DLPE (41.0 Å^2 and 49.1 Å^2, respectively) [39]. The cylindrical construction with a diameter approaching 48 Å leaves a central hole large enough to accommodate the peptide with its hydrophobic portion, from Ala7 to Phe21, correctly inserted between the two planes of the carbonyl groups of the acyl chains separated by 26 Å.

The lipid/peptide system was immersed in a cylinder of 3026 TIP3P water molecules previously equilibrated during 5 ps at 300 K. The excess water molecules were removed in successive steps. First, water molecules located between the two planes of the carbonyl groups of the acyl chains were deleted leaving two hydration layers

with a thickness of 13 Å beyond the phosphate planes which is sufficient to hydrate phosphatidylcholine bilayers, well above 5 Å needed to hydrate phosphatidylethanolamine bilayers [40]. Second, water molecules within a distance of 2.3 Å from the lipid and peptide atoms and water molecules farther than 24 Å from the helix axis (X axis of the system) were discarded to give the final cylindrical shape of the system. The resulting bilayer model is composed of 5560 atoms including 1036 water molecules and includes approximately 20 waters per lipid. According to Woolf and Roux [41], the presence of 20 explicit water molecules around the polar group is sufficient to reproduce qualitatively the behavior found in bulk water.

2.3. Constraints applied to the system

A cylindrical stochastic potential constituted by a slightly attractive and a strongly repulsive part was used to maintain water and lipids within a radius of 24 Å from the central axis of the system. This spline-based solvent boundary potential [42] was applied to the second aliphatic and terminal carbon atoms of the acyl chains and to the water oxygen atoms. A similar spherical boundary potential centered very far away from the simulated system to mimic planar boundaries was applied on the two hydration layers to prevent water escape.

2.4. Simulation parameters

The simulations were performed with the X-PLOR program (version 3.1) [43]. Parameters were taken from the CHARMM extended carbon atom force field (param 11 and param 19) [44]. The partial charges on DLPE atoms given in Table 1 were obtained from semi-empirical calculation using MOPAC/MNDO93. They are similar to those used by Damodaran [45], except for N atoms bearing a strongly negative charge, but the complete NH_3 group was positively charged with a net charge of approximately 0.6 in both cases. The three basic residues at the C-terminal side of the peptide were considered without net charges to account for the absence of counter ions in our model.

According to the united-atom representation, only polar hydrogen atoms of the peptide and of the lipids were kept. A dielectric constant of 1, a shifted electrostatic function with a cutoff value of 11 Å and a smooth switching function over 1 Å for van der Waals interactions were used. The 1–4 electrostatic interactions were scaled by an ϵ1-4 factor of 0.4 compatible with the force field parameters used. The atom pair list was automatically recalculated considering a distance of 12 Å for non-bonded list generation and a tolerance of 0.5 Å [43].

2.5. Initial configuration for MD start

The starting configuration was energy minimized in successive runs for several hundred steps of conjugate gradient [46] to suppress steric contacts between the peptide, lipids and water atoms. The first minimization run was performed subject to weak distance restraints at the first and the last helix turn in order to avoid helix end disorder at the membrane interfaces. We have shown that such weak constraints at helix termini do not affect the dynamics of the peptide under vacuum conditions [34]. For the second minimization run, a smooth restraining potential was added between the two last methyl carbon atoms of the acyl chains of each outer lipid keeping them at a distance of approximately 7 Å. These constraints were maintained during the simulations to prevent a too large lipid disorder near the cylindrical wall. Constraints at helix extremities were also maintained. After these two minimization stages, steric contacts disappeared without affecting the helical peptide structure.

2.6. MD protocol

2.6.1. In membrane environment

The resulting minimized structure was slowly heated to 300 K in steps of 50 K, each during 4 ps. New atomic velocities taken from a Maxwell distribution were assigned at each temperature step. At 300 K the temperature of the system was

Table 1
Atomic point charges for DLPE

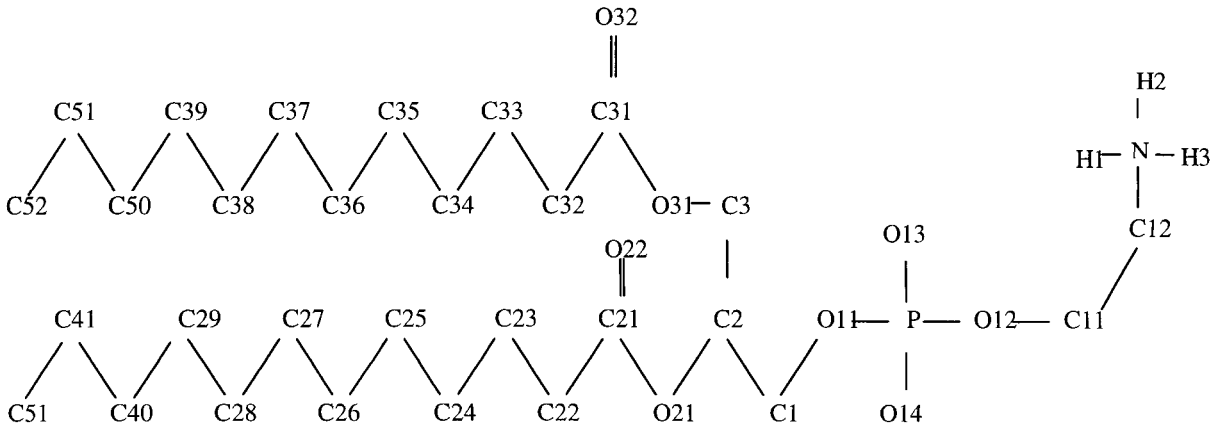

Atom	Charge	Atom	Charge	Atom	Charge
H1	0.220	O21	−0.320	O31	−0.345
H2	0.220	C21	0.363	C31	0.360
H3	0.220	O22	−0.364	O32	−0.362
N	0.028	C22	0.060	C32	0.070
C12	0.120	C23	0.030	C33	0.040
C11	0.260	C24	0.005	C34	0.005
O12	−0.570	C25	0.000	C35	0.000
P	1.360	C26	0.000	C36	0.000
O13	−0.690	C27	0.000	C37	0.000
O14	−0.800	C28	0.000	C38	0.000
O11	−0.540	C29	0.000	C39	0.000
C1	0.220	C40	0.000	C50	0.000
C2	0.170	C41	0.000	C51	0.000
C3	0.240	C42	0.000	C52	0.000

further increased to 315 K in 5 ps with a new velocity assignment every 1 ps. This temperature of 315 K is well above the gel–liquid crystalline phase transition temperature of 303.5 K [47]. The system was equilibrated during 50 ps with a friction parameter equal to 100 ps^{-1} on all atoms, then during 75 ps with a value of 50 ps^{-1} and finally the last 25 ps with a value of 20 ps^{-1}. The SHAKE algorithm [48] was applied and a time step of 2 ps was used. The whole process of the heating and equilibration periods (over 150 ps) was repeated with different initial atomic velocities leading to two final equilibrated conformations taken as starting structures for two different 500-ps MD simulations. Coordinates were stored every 0.4 ps to generate two trajectories referred to as MD1 and MD2 in the following.

2.6.2. In vacuum

The MD protocol applied to generate in vacuum trajectories for the same wild sequence was previously described [34]. The two trajectories therein referred to as MD^v6 and MD^v7 are used for comparison with the results of 'in lipids' simulations presented here.

2.7. Trajectory analysis

The helix structure was probed from HB time series generated using the PROMHB module of

GROMOS. Criteria for HB existence are that the distance between the donor (D) and the acceptor (A) atoms is smaller than 0.35 nm and that the DHA angle value ranges from 135 to 180°. In order to underline large amplitude variations, a smoothing technique was applied to plot HB and energy time series.

To follow the dynamics of the peptide, time autocorrelation functions of covalent bond vectors of all the residues were computed. The $C\alpha$–$C\beta$ vector was considered for the backbone dynamics and the $C\beta$–$C\gamma$, $C\gamma$–$C\delta$, $C\beta$–$O\gamma$, ... were considered for the side chains.

The calculated autocorrelation function corresponds to

$$A(t) = \left\langle \frac{3\cos^2\theta i(t) - 1}{2} \right\rangle$$

where $\theta i(t)$ is the angle between the direction of a vector at times T and $T+t$, respectively. The angle brackets represent an average over T along the trajectory. $A(t)$ is comprised between 1 and -0.5. In the Lipari–Szabo [49,50] formalism often used to calculate these autocorrelation functions, a plateau different from 0 is reached when the motion is restricted to a limited area.

2.8. Bilayer analysis

The membrane behavior was characterized by the electron density distribution normal to the membrane and distribution of water molecules around the lipid polar heads.

The electron density profile $e(x)$ along the bilayer normal (X axis) was calculated as

$$e(x) = \left\langle \sum_{\sin V}^{\text{all atoms}} ne(x)/V \right\rangle$$

$ne(x)$ is the number of electrons associated to one atom within the volume V comprised between two parallel planes located at x and $x + 0.5$ Å. The number of electrons assigned to one atom is the atomic number minus its partial charge. The brackets represent an average over a given period of the simulation.

The hydration of lipid head groups was probed by evaluating the radial distribution function $g(r)$ of water oxygen atoms around phosphorous, nitrogen and carbonyl carbon atoms. $g(r)$ was expressed as $g(r) = \mathrm{d}N(r)/4\pi r^2 \mathrm{d}r\rho_o$, where $\mathrm{d}N(r)$ is the number of water oxygen atoms comprised between two concentric spheres of radius r and $r + \mathrm{d}r$ centered on the reference atom (r ranging from 0 to 10 Å and $\mathrm{d}r = 0.05$ Å) and ρ_o is the number of water molecules of the total volume of the simulated system.

3. Results

3.1. Full system

The minimized starting configuration used to produce the two 500-ps simulations (MD1 and MD2) and the resulting structures obtained after 100 ps of equilibration at 315 K are displayed in Fig. 1a–c, respectively. During equilibration, the water molecules remain confined within the applied boundaries and the global cylindrical shape is conserved. Consistent with the liquid crystalline phase some transitions occur in the aliphatic chains of the lipids.

The stability of the potential energy of the full system has been checked in the two simulations. In both cases a very small drift, essentially due to variations in electrostatic interactions at the membrane interfaces, is observed (0.8% for MD1 and 0.5% for MD2). van der Waals energy remains remarkably stable. Fig. 2 shows snapshots of the system at the end of the two 500-ps production periods. Water molecules penetrate the bilayer to hydrate the lipid glycerol groups and no diffusion of water within the hydrophobic core of the fatty chains is observed. The chains become slightly disordered during the simulations but the lipid configurations remain consistent with that usually observed [51] compatible with what is expected for the liquid crystalline phase of a DLPE bilayer at 315 K. The lipids of the inner ring match the hydrophobic portion of the peptide and ensure a stable environment during the whole production period.

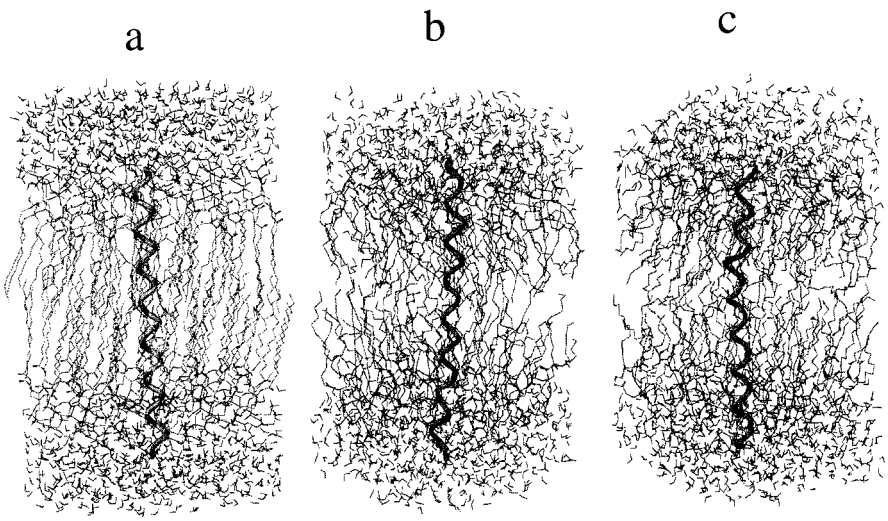

Fig. 1. (a) Mininmized structure of the wild ErbB-2 transmembrane helix embedded in a fully hydrated L-α-dilauroylphosphatidylethanolamine (DLPE) bilayer used as the starting configuration for MD1 and MD2 simulations. (b) Snapshot of the full system after 100 ps of equilibration at 315 K showing the α helix structure of the peptide observed in MD1. (c) Snapshot of the full system after 100 ps of equilibration at 315 K showing a π deformation at the mutation site in MD2. The ErbB-2 transmembrane helix is shown as a thick tube.

3.2. Membrane behavior

Our simple model for representing the lipid environment raises the question of the lipid bilayer behavior. To evaluate possible distortions of the membrane due to the cylindrical boundary conditions, we have first calculated the electron

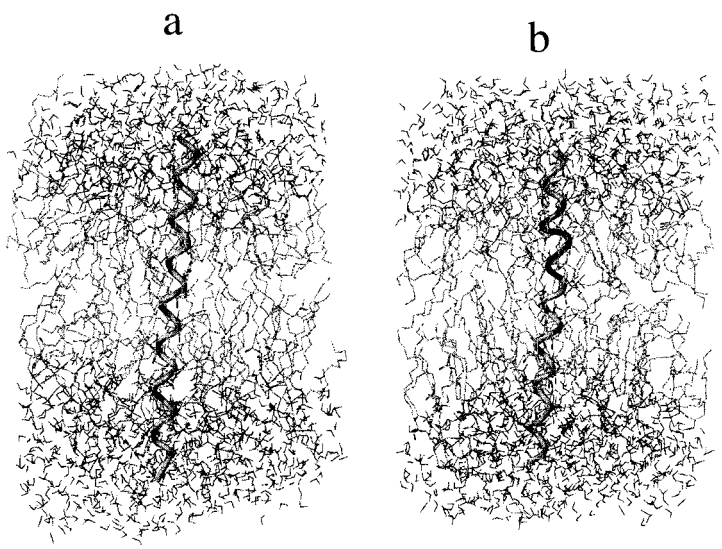

Fig. 2. Snapshots of the lipid/peptide/water system after 500 ps of production at 315 K. (a) The α helix is maintained in MD1. (b) The π deformation at the mutation site is still present in MD2 and covers 5 π HB. As in Fig. 1, the ErbB-2 transmembrane helix is shown as a thick tube.

density profile $e(x)$ along the bilayer normal averaged over the last 200 ps of the production phase of the simulation. The total electron density profile and the separate contributions of lipids and water are shown in Fig. 3. The highest peaks of the overall density coincide with the maximum of the density profile of the phosphate and amine groups. The distance between the two peaks is approximately 31 Å and this is in correct agreement with the values experimentally obtained for the liquid crystalline phase (33.0 ± 0.6 Å) [39]. The shoulder of the peaks corresponds to the maximum of the lipid contribution which is also the maximum of the ester groups electron density profile (not shown). The water electron density has its maximum at ± 21.3 Å and decays to zero after the phosphate groups and the glycerol ester region. The trough in the total electron density corresponds to the terminal methyl region. This low density region is consistent with the experimental observation and shows that the two monolayers do not move apart during the simulation. This profile also confirms that the transmembrane helix remains in close proximity with the lipids.

The width of the bilayer and of its hydrocarbon core can be estimated from the total density profile, using the definitions given by McIntosh and Simon [39], to 39 ± 1 Å and 21 ± 1 Å, respectively. Given the error bars on the estimations,

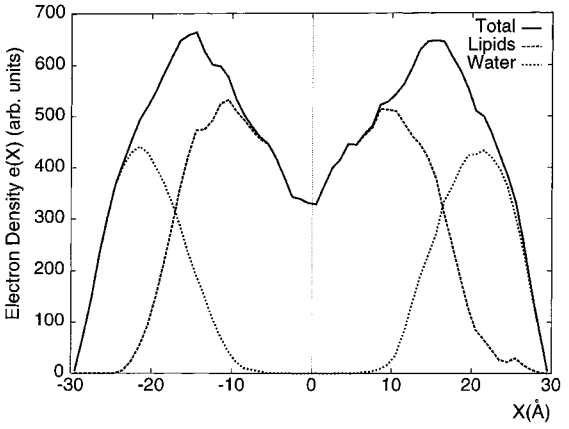

Fig. 3. Total electron density profile along the bilayer normal and contribution of lipip and water molecules averaged over the last 200 ps of MD1.

these values are very close to those measured experimentally (41 ± 0.6 Å and 23 ± 0.6 Å) [39]. This result, in addition to the analysis of the electron density along the bilayer normal shows that our simple DLPE model bears experimental features characteristic of the lipid crystalline phase of the DLPE bilayer and clearly demonstrates that the stochastic boundary conditions do not induce significant distortions.

The radial distribution functions of water oxygens about the lipid atoms have been calculated to probe the hydration of the polar head groups. As an example, the radial distribution functions of water about the phosphorous and nitrogen atoms are given in Fig. 4. The P–O (wat) $g(r)$ function has a maximum at 3.725 Å and the primary hydration shell around P atoms (measured as the integral of $g(r)$ up to its first minimum at 4.85 Å) is constituted of 8.3 water molecules. The N–O (wat) $g(r)$ function shows a sharp peak at 2.8 Å and a first minimum at 3.6 Å. The primary hydration shell around the N atoms is constituted of 4.3 water molecules. The positions of the peaks in the P–O (wat) and N–O (wat) $g(r)$ functions are very similar to those obtained from DLPE lipid bilayer simulations with periodic boundary conditions [45]. Approximately 12 water molecules are associated to one lipid which is quite a good estimate compared to 10 waters per lipid estimated from experiments [39,40], and to 15 waters per lipid estimated from simulations under periodic boundary conditions [45]. The remaining eight water molecules per lipid and the solvent stochastic potential [42] applied on each side of the bilayer model, constitute the bulk solvent.

These results show that our model is quite reasonable and reproduces features that are characteristic of the liquid crystalline phase of the DLPE bilayer. This gives confidence in the dynamic features of the ErbB-2 transmembrane helix.

3.3. Peptide structure

3.3.1. Equilibration periods

The structure of the peptide is shown in Fig. 1b as it appears at the end of the equilibration

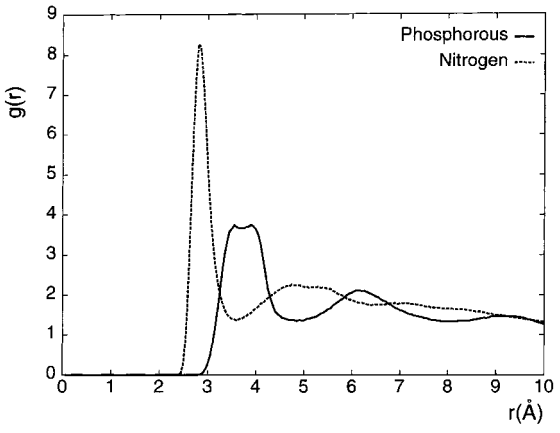

Fig. 4. Radial distribution functions of water oxygens about the phosphorous and the nitrogen atoms of the MPE head groups averaged over the last 200 ps of MD1.

period of MD1. The peptide retains its regular α helical conformation characterized by a complete hydrogen bond network between the carbonyl groups of residues i and the amide groups of residues i + 4. On the contrary, the peptide observed at the end of equilibration of MD2 (Fig. 1c) is helical but over the 26 i i + 4 potential HB that lock the complete α helical structure, only 24 exist. At the oncogenic mutation site, two i i + 4 HB, namely CO8–NH12 (8–12) and CO9–NH13 (9–13) are disrupted and replaced by two others involving the CO groups of residues i and the NH groups of residues i + 5 (7–12 and 8–13). This characterizes an incipient π helix. At this stage of equilibration the 7–12 π HB exists as a bifurcated HB with the 7–11 α HB. The rupture of the 9–13 α HB liberates the carbonyl group at the Val9 site. This π deformation is viewed on the tube diagram as a wide helical turn consistent with a local unwinding of the helix.

3.3.2. Production periods

Fig. 2a,b shows snapshots of the peptide embedded in the bilayer model at the end of the 500-ps production periods for MD1 and MD2, respectively. In MD1, the whole α helical structure is maintained whereas in MD2 we observe an increase of the length of the π deformation up to 5 π HB.

The time evolution of the backbone HB network over the 500 ps of MD2 is shown in Fig. 5. During the first 25 ps, the backbone HB network is conserved with the free CO9 group and the bifurcated 7–11 and 7–12 HB. After 100 ps, a third π HB appears (6–11) concomitant with the total rupture of the 7–11 α HB. The new N-terminal boundary of the π bulge consists of the bifurcated HB including 6–10 and 6–11. By the same cooperative process, a fourth π HB (5–10) is transitorily formed between 100 and 300 ps and then locked. The strong 5–10 HB formation is correlated with the disruption of the 6–10 α HB. Finally, between 300 and 500 ps, the destabilization of the 5–9 α HB is observed simultaneously with the formation of the 4–9 π HB leading to a π bulge of 5 π HB in length at the end of the simulation. The carbonyl CO9 group remains free and does not participate in HB interactions with the peptide or lipid atoms during the overall simulation. The rest of the peptide displays the typical α helical HB network. The successive π HB formation induces several distinct states of the helical structure as shown from the variations of the root-mean-squared deviations (RMSD) of the peptide coordinates calculated from the initial configuration with time (Fig. 6). RMSD values are calculated vs. the first configuration of the trajectory.

Fig. 7 shows, for comparison, the time series of the α and π backbone HB extracted from the simulation performed in a vacuum for the wild type of the transmembrane domain previously named MD^{v}7 [34]. During this simulation, a 4 π HB deformation appears within the α helix 100 ps after the end of equilibration. We determined that the transition is initiated when the 7–12 π HB is spontaneously formed. Then the deformation extends towards both the N- and C-extremities according to the mechanism previously detailed [35]. Towards the N-terminus, two additional π HB (6–11 and 5–10) are formed, similarly to those occurring in the membrane environment, with a tendency to the reappearance of the αHB for the 5-10HB. Only one additional π HB is formed at the C-terminal side (8–13) leaving the CO9 carbonyl group free without HB interactions with the peptide, lipids or water. In both environments, the π bulge extends over the same portion of the peptide ranging from residue 4 to residue

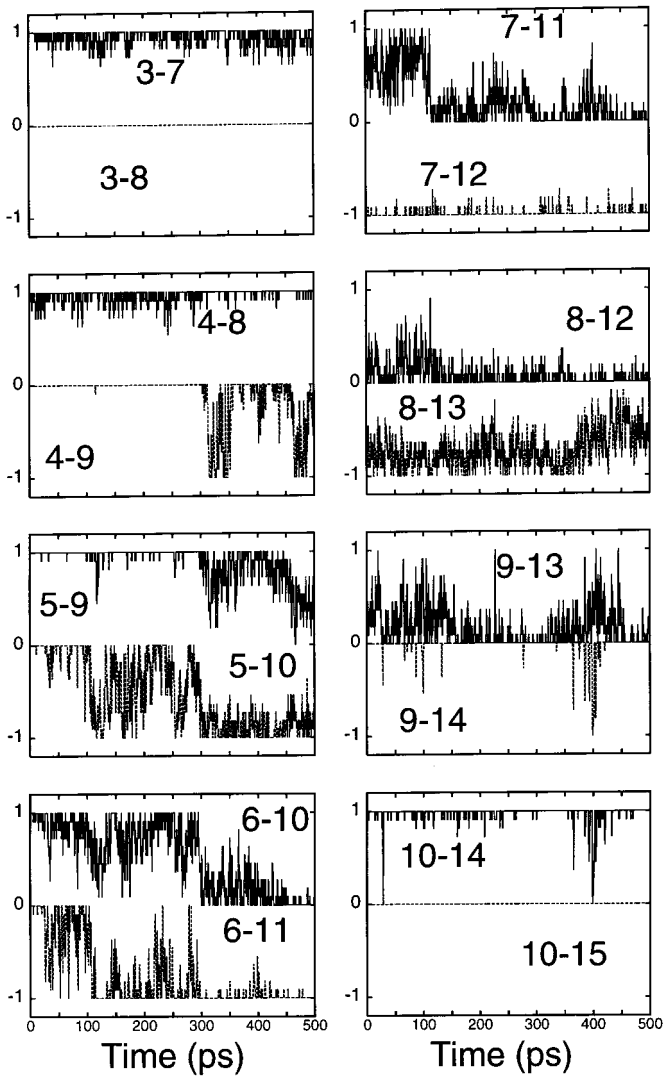

Fig. 5. Backbone HB time series of the ErbB-2 transmembrane helix in a membrane environment (MD2) showing the propagation of π HB formation. In ordinate, the value 1 indicates the presence of a α HB (noted by the residue numbers ii + 4), the value -1 indicates the presence of a π HB (noted by the residue numbers i i + 5), the value 0 means that no HB is formed. The smoothing technique used (window of 11 elements) for the plots explains intermediate values.

13. In a vacuum, the propagation of the deformation towards the N-terminus occurs within a few picoseconds whereas it takes at least 300 ps in a membrane environment. The C-terminal propagation observed in the vacuum is not detected in the lipid environment.

3.4. Correlation functions

The 'in lipids' MD1 simulation and the first 500 ps of the in vacuum MD^{v}6 simulation were used to characterize the α helix backbone. MD2 (in membrane) and MD^{v}7 (in vacuum) served to characterize the motions of the helix backbone when it experiences π deformation.

3.4.1. Backbone motions

The dynamics of the backbone part of the TM helix was analysed by evaluating the autocorrela-

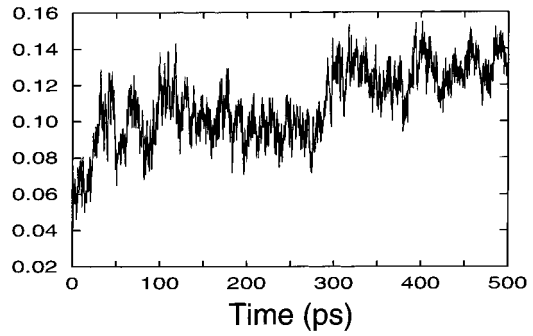

Fig. 6. Coordinate root mean square deviations (rmsd, in nm) between the structure obtained at time t (abscissa) and the initial structure during the 500-ps molecular dynamics trajectory MD2. The steps in rmsd values are correlated to the formation of π H-bonds shown in Fig. 5.

tion functions of the Cα–Cβ vectors for all residues. The curves (not shown) exhibited little variation with the residue number and were thus averaged over all residues to improve accuracy.

In the case of the α helix (MD1 and MD^{v}6), the autocorrelation functions exhibit a very weak decrease and converge in a few picoseconds towards the value of 0.95 in a membrane environment and 0.90 in a vacuum. This weak decrease indicates that the backbone motions are strongly limited in both environments, in agreement with the almost identical value of the root-mean-square (rms) of the ϕ and ψ dihedral angle fluctuations calculated for the two simulations (10° in vacuum and 9° in membrane). The same weak decrease of the autocorrelation functions is observed when the helix undergoes π deformation (MD2 and MD^{v}7).

3.4.2. Side chain motions

Rms fluctuations of χ_1 dihedral angles for all residues are shown in Fig. 8. In a vacuum, the rms values are generally high, particularly for residues undergoing numerous χ_1 transitions. In contrast, in the membrane, χ_1 transitions are much less frequent giving rise to low rms values. To further compare the side chain motions in the two environments in relation to the helix structure, the autocorrelation functions of the Cβ–Cγ1 vector of Val and Ile residues and of the Cβ–Oγ vector of Thr2 (13 β-branched residues), were calculated. Autocorrelation functions for some of these residues, representative of all side chain motions, are shown in Fig. 9.

The side chain motions are examined when the helix remains in the α structure, in vacuum (MD^{v}6) and in an explicit lipid environment (MD1) (Fig. 9a). In most cases, the autocorrelation functions exhibit a rapid initial decrease followed by a plateau at approximately 0.8 (vacuum) and 0.9 (DLPE). The corresponding amplitude of the angular displacement of the vectors is estimated at 21 and 15°, respectively, according to the Lipari–Szabo formalism. This indicates a very restricted motion generally observed for the Val side chains as exemplified for Val9. The same kind of motion is observed for residues like Ile23, at the C-terminal extremity of the peptide. The Val19 side chain shows a larger angular amplitude, estimated at approximately 40° in vacuum, reflecting the frequent χ_1 transitions. A major damping of the motion of this side chain is observed in the membrane, also visible in the case of the Thr2 side chain. This side chain protrudes into the hydration layer and is largely hydrated all along the simulation. Only a few interactions with the polar head groups are detected. The corresponding autocorrelation function shows that, in a vacuum, a plateau (order parameter) of approximately 0.6 is rapidly reached, and is significantly smaller than 0.85, measured when the peptide is embedded in the bilayer.

To evaluate the effect of the backbone structure on the side chain motions, the autocorrelation functions were compared between simulations MD1 and MD2, in the bilayer environment, on the one hand, and between simulations MD^{v}6 and MD^{v}7, in a vacuum, on the other hand,

For nine residues out of the 13 β-branched residues considered, simulations MD1 and MD2 lead to very similar autocorrelation functions (Fig. 9b), such as that shown for Ile5. Globally, the side chain mobility is not strongly affected by the helix deformation. The angular displacement of the Cβ–Cγ bonds remains relatively constrained as attested by the value of the plateau at 0.8–0.9. However, for residues Val8, Val14 and Val16, some differences in mobility are detected as shown for Val16, and also, for Ile4 with slightly larger

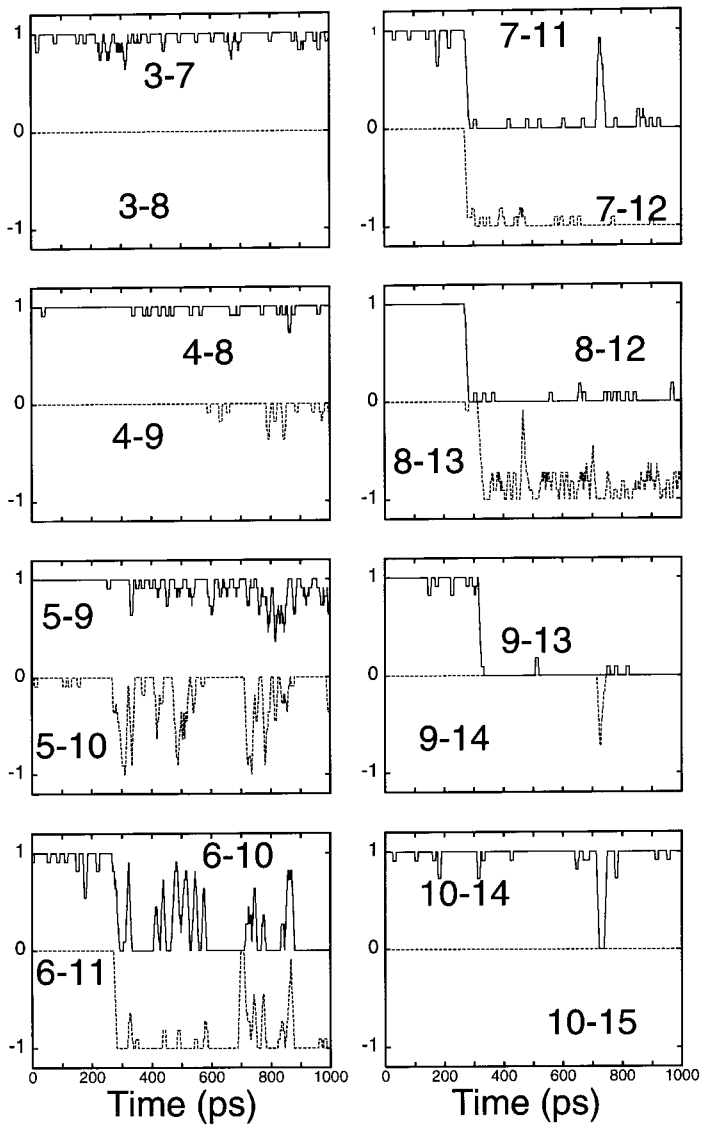

Fig. 7. Backbone HB time series of the ErbB-2 transmembrane helix showing the π deformation occurrence in the vacuum simulation MD^{v}7 (same as in Fig. 5).

angular motions in the altered helix, as confirmed by higher rms values. However, the number of transitions remains low (only 16 transitions are detected in MD2 for the whole set of the β-branched residues), and the observed differences could also be the result of a miss averaging over the 500-ps time scale. A potential coupling between the motions of the side chains and the motions of the backbone cannot be clearly evidenced from the simulations.

The same autocorrelation functions calculated from in vacuum simulations (MD^{v}6 and MD^{v}7) (Fig. 9c), reveal two different behaviors. Five residues (including residues 2, 11, 20, 23, 25) out of the 13 residues considered show a very similar side chain mobility when the helix keeps its α

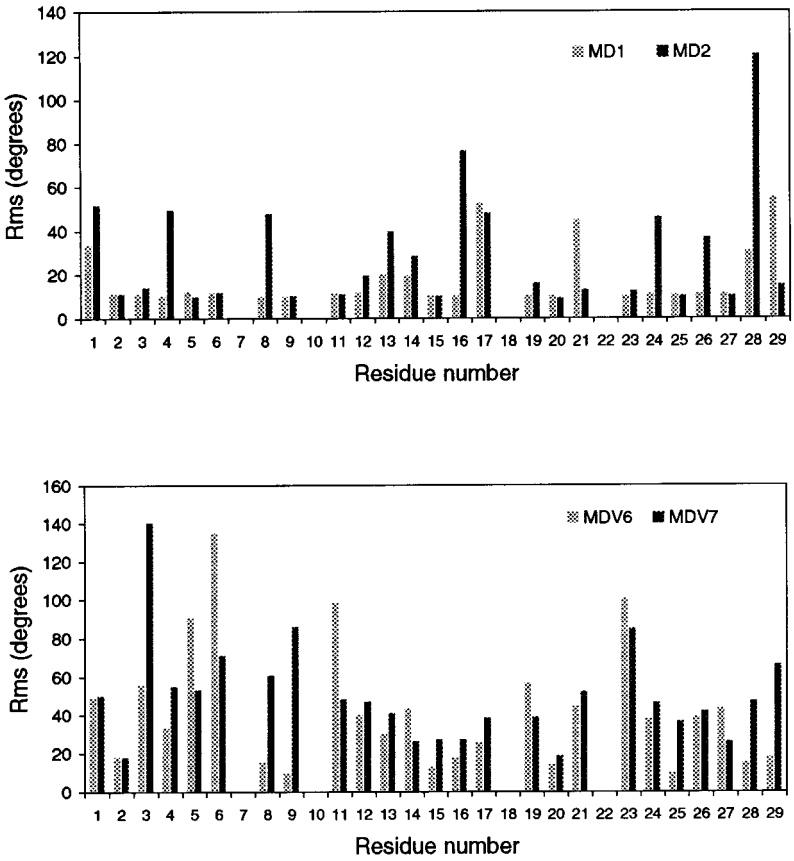

Fig. 8. rms fluctuations of χ_1 side chain dihedral angles during molecular dynamics simulations. Top: in membrane, α helix structure (MD1, 500 ps), π altered helix (MD2, 500 ps). Bottom: in vacuum, α helix structure (MD^v6, first 500 ps), π altered helix (MD^v7, 1 ns).

structure and when it is π deformed. This is illustrated for Ile11. For the eight other residues, a slightly larger decrease of the autocorrelation functions is observed when the α helix is altered. This behavior is illustrated for Val8.

In summary, π helix alteration noticeably increases the dynamics of the side chains in vacuum, leading to larger χ_1 fluctuations for residues located within the π deformation area. When the peptide is embedded in a DLPE membrane, the motions of the side chains are strongly reduced, masking a potential effect of the helix backbone deformation.

3.5. Energetic study

The internal energy of the peptide in the α helical structure (MD1) is approximately 12 kcal mol^{-1} on average, below the internal energy of the altered helix (MD2) (Fig. 10). The difference in stability comes both from van der Waals and electrostatic interactions. The π deformation leads to less favorable electrostatic interactions (approximately 15 kcal mol^{-1}) probably due to weaker π HB interactions and to the absence of the α 9–13 HB, but also to more favorable van der Waals energies reaching almost 20 kcal mol^{-1}

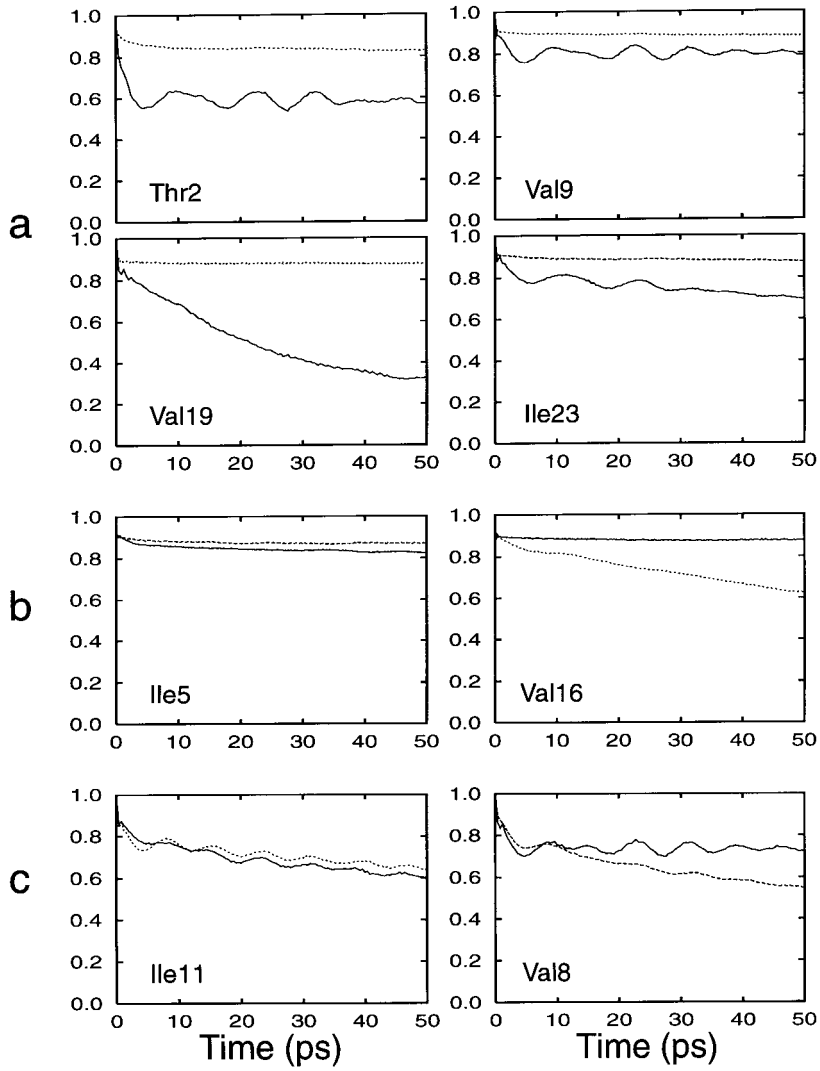

Fig. 9. Autocorrelation functions of the Cβ–Cγ (or Cβ–Oγ) vectors illustrating different type of side chains motions. (a) Thr2, Va19, Val19, Ile23: α helix structure, in vacuum (MD^{v}6 (———), first 500 ps) and in membrane environment (MD1 (...), 500 ps). (b) Ile5, Val16 in a membrane environment, α helix structure (MD1 (———), 500 ps), π altered helix (MD2 (...), 500 ps). (c) Ile11, Val8: in vacuum, α helix structure (MD^{v}6 (———), first 500 ps), π altered helix (MD^{v}7 (....), 1 ns)).

during the last 200 ps of MD2. These same observations have been reported from our analysis of simulations performed in vacuum using the GROMOS or CHARMM force field.

3.5.1. Lipid and water effect on the α helix

It is interesting to analyze the effect of the different components of the bilayer on the embedded peptide. The water–peptide interactions, between -300 and -350 kcal mol^{-1}, are relatively strong compared to the lipid–peptide interactions, approximately -200 kcal mol^{-1}. The analysis of the interaction forces applied on the peptide indicates that the forces induced by water molecules are twice as strong as those induced by the lipids but their distribution along the peptide varies according to the nature of the residues (Table 2). The transmembrane peptide can be

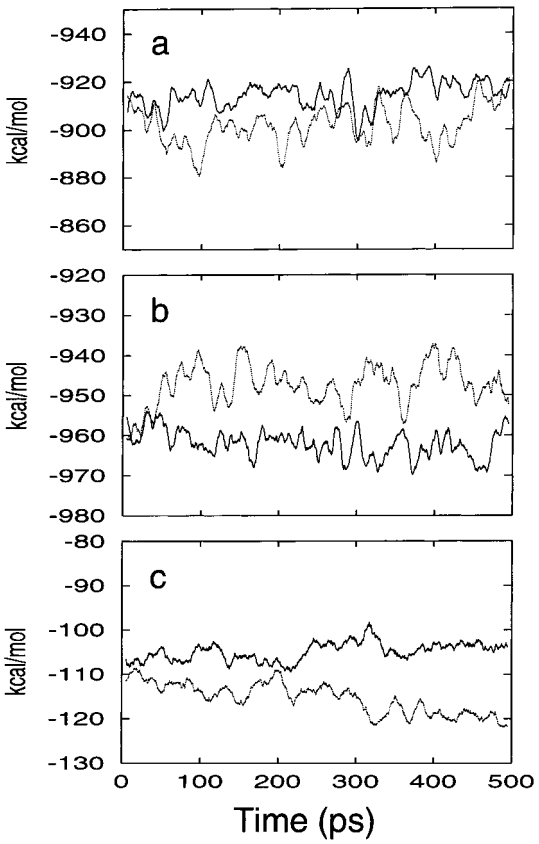

Fig. 10. Smoothed time series (window of 11 elements) of the intramolecular energy of the peptide embedded in a hydrated DLPE bilayer: MD1 (———) and MD2 (...) simulations. (a) potential energy; (b) electrostatic energy; (c) van der Waals energy.

divided in three parts: (i) the N-terminal part (residues 1–6) describes a first hydrophilic juxtamembrane portion; (ii) the intramembrane part (residues 7–24) is the hydrophobic core; and (iii) the C-terminal part (residues 25–29) corresponds to the other hydrophilic juxtamembrane portion. Table 2 shows that the forces exerted by water, essentially due to long range electrostatic interactions with polar backbone atoms, are four to five times stronger at the helix termini than at the hydrophobic core. On the contrary, the lipid contribution is almost equally distributed along the three peptide parts although the forces applied at the C-terminal extremity are slightly stronger due to the presence of polar residues. The forces exerted by the lipids on the peptide hydrophobic core are of the same order of magnitude as those exerted by the water molecules but are predominantly of van der Waals nature. At this level of the transmembrane helix, the major contribution of the forces (70%) originates from intrapeptide interactions.

4. Discussion

The aim of this study was to probe the effect of an explicit lipid environment on the structure and the dynamics of the ErbB-2 transmembrane domain.

From a series of 1-ns molecular dynamic simulations performed in vacuum on the wild sequence and on different mutants (Val659 replaced by Gly, Asp, Glu or Gln), we previously demonstrated that the α helix experiences local π deformations [34]. This structural phenomenon was systematically reproduced under different conditions of simulations. Nevertheless, the vacuum approximation used to simulate the motions of the transmembrane peptide remained questionable.

In the present study, we address this point by analyzing the results of two 500-ps simulations of the wild transmembrane peptide in a membrane model composed of a fully hydrated DLPE bi-

Table 2
Forces applied on the ErbB-2 transmembrane peptide

Forces	Peptide/water	Peptide/lipids	Intra-peptide
N term (Leu1–Ala6)	12.9	3.5	10.2
Core (Va17–Leu24)	2.5	2.0	10.2
C-term (Ile25–Gln29)	10.0	4.2	10.2

Note. The contributions of water and lipid molecules are normalized over the number of atoms contained in each of the three distinct parts of the peptide. The intramolecular forces exerted on the peptide are calculated for all the atoms (in kcal/mol/Å).

layer. One simulation shows that the peptide remains in the regular α helix structure and the second one shows that the α helix undergoes a π deformation initiated at the same site as observed in vacuum. These results are not contradictory. In the vacuum, we found that the appearance of the first π HB arises after at least 500 ps on average. It is reasonable to think that this time should be much longer within an explicit membrane environment and that π alterations would have been observed in the first simulation, too, for longer simulation times.

The formation of additional π HB towards the N-terminus occurs according to the same mechanism described from our previous in vacuum simulations [35] and corresponds to the successive replacement of α HB by π HB resulting in a deformation of 5 π HB in length at the end of the simulation. Even for this short π deformation, the structural consequences are very important. A register shift is induced by the π bulge formation which results in a helix unwinding approximately 100° and changes in the helix faces. β-Branched residues, often in successive arrangement in the sequence, were previously shown to be a crucial determinant for the $\alpha \rightarrow \pi$ transition. The steric contacts that they generate within the α helix are relaxed through the effect of the local helix unwinding and lead to van der Waals stabilization. This gain in stability is also observed when the peptide is immersed in a hydrated bilayer and reaches 20 kcal mol^{-1} for four or five successive π HB. Similar changes in electrostatic interactions associated to the π deformation are also observed in both environments.

The internal dynamics of the peptide involves global peptide motions such as the overall helix deformation and local motions such as the side chain dynamics. We have shown that the essential difference between vacuum and explicit membrane environment is the time scale of the propagation of the π deformation. In our membrane model, 100 ps are necessary on average to form a new πHB whereas 10 ps are sufficient on average in a vacuum. Furthermore, the π HB propagation towards the C-terminus has not been observed in the present simulation but it is often seen as a slow rate process in a vacuum. This is probably due to a too short 500-ps time scale relative to the slowing down of the propagation. In addition, we already demonstrated that, in vacuum, the C-terminal propagation often fails to overcome Gly residues because of their flexibility. Generally, Gly is located at the junction of the α HB and π HB networks. In membrane simulation, this feature is also reproduced.

The present work also shows that the structural behavior of the backbone is not affected by the membrane environment, but that the dynamics are slowed down, very probably through the effect of the coupling between the backbone and the side chain motions, generally found more constrained. Interactions between the backbone atoms of the hydrophobic core and water are weak and come essentially from electrostatic interactions that act on polar atoms. On the side chains, the electrostatic contribution is null and their restricted motions, observed in explicit membrane, are only a consequence of van der Waals interactions. At the two N and C helix ends, where hydrophilic residues are present, the membrane interface contributes to a further decrease of atomic fluctuations owing to more complex interactions involving both van der Waals and electrostatic contributions with the polar head groups and water molecules.

As a global result, the tendency for the peptide backbone at the hydrophobic core is to behave similarly in vacuum and in membrane environments, but the different behaviors observed for the side chains make the vacuum approximation inappropriate to describe their dynamics.

The fact that the transition is initiated at the same site within the helix core and is propagated according to the same mechanism in both environments demonstrates that the lipid proximity does not modify the conformational space accessible to the helix. Therefore, the vacuum environment emphasized as extremely hydrophobic [52,53] can reasonably be used to explore the conformational space of the hydrophobic part of transmembrane domains on a large time scale. Moreover, the $\alpha \rightarrow \pi$ transition extends from Ile4 to Val13 including some residues lying in a more hydrophilic environment. At this level, where water and polar head groups may interact

with the peptide, the π deformation seen in vacuum is also reproduced within the explicit membrane. This result is rather unexpected owing to the different properties of the two environments. Therefore it could be hypothesized that the intrinsic structural properties of the transmembrane peptide, as they are characterized in vacuum, dominate the environmental effects even when it becomes more hydrophilic [52].

To date, few simulations on peptides inserted in an explicit bilayer have been reported [54–59]. Shen and collaborators have analyzed the stability of a single homogeneous alanine helix immersed in a hydrated dimyristoylphosphatidylcholine (DMPC) bilayer and in vacuum. Very interestingly, they show the existence of the π helix for a length of time almost equivalent to that spent in the α form in vacuum and a smaller π helix percentage in membrane. Recently, dynamic simulations of individual helices of bacteriorhodopsin in a hydrated DMPC bilayer have shown the appearance of short π structures within some helices [58]. In a similar lipid environment, they are also detected in the transbilayer- synthetic peptide including a leucine-rich hydrophobic part [59].

Subtle π deformations in the ErbB-2 transmembrane segment have not been evidenced from the structural studies published to date [33,60]. However, as widely discussed [34], π helix deformations are not rare and are observed in the high resolution crystal structure of soluble proteins and membrane proteins. Therefore the presence of such alteration in ErbB-2 TM is interesting in discussions relating to biological activity.

The activation process of many cell surface receptors is triggered by dimerization [61] and, in the case of the ErbB-2 receptor, it is demonstrated that the oncogenic Glu mutation is involved in dimer formation [33]. A better understanding of receptor dimerization and particularly of the interactions governing the transmembrane helix dimers lead us to propose atomic models on the basis of theoretical modeling and MD simulations [62]. We have shown that the wild and the Glu mutated dimer structures use the same helix faces for the best contacts with an increased stabilization by direct hydrogen bonding between the Glu side chains. An interesting fact is that the formation of the dimer is accompanied by a π deformation for one of the two helices and very often observed at the site essential for cellular transformation. The change in the properties of helix faces is the most dramatic consequence of α helix alteration and could play an important role in the whole receptor function. Transmembrane helix plasticity in a membrane medium is very often suggested from theoretical studies and this property might be used to favor best contacts for optimizing helix–helix interactions.

The π bulge model could help to interpret the results of mutational experiments that cannot be explained in the context of a canonical α helix [63,64]. In the case of the rat neu protein (homologous to ErbB-2), it is shown that Glu664 flanked by Val663 and Gly665 are absolutely required to maintain the transforming potency of the transmembrane domain. Since these three successive residues cannot participate together in helix packing, one possible interpretation would be to associate a structural alteration with the mutations. This interpretation would also explain why a non-transforming effect is obtained when the same VEG triplet is shifted at one or two turns after the mutation site on the same face of a canonical α helix. This suggests that either the mutations suppress possible additional interactions necessary for the transforming effect or that the triplet is not correctly located on the helix faces to form a dimer.

5. Conclusion

One of the most important causes of misinterpreting the results of MD simulations of biomolecules is the lack of a correct averaging over the configuration space. A good estimate of transitory phenomena with 95% confidence would require the reversibility of the transition (system at equilibrium) and a simulation time scale 20 times larger than the mean time associated with its observation [65]. Therefore, the unambiguous description of structural transition arising well over 1 ns would be out of range to date in an explicitly lipid environment.

In the present work, we have demonstrated

that in a DLPE bilayer model, water molecules and lipids have only a small influence on the configurational space available to a transmembrane peptide in the core of a membrane on a 1-ns time scale. This is mainly because most of the stability of the peptide comes from internal hydrogen bonds. Compared to in vacuum simulations, the time explored in the membrane model is too short to observe important rotamer transitions of the side chains mostly hindered by the presence of the lipid chains. Therefore, vacuum simulations appear like a cheap tool accurate enough to have access to important information on the internal deformation of a hydrophobic peptide. However, they must be completed by simulations in an explicit solvent and lipid environment when one is interested in the details of the peptide dynamics or in interactions with other peptides. Such interactions are particularly important for peptides susceptible to form dimers like the ErbB-2 transmembrane domain.

From our series of simulations and the analysis of transmembrane domains of a few crystallized membrane proteins, it emerges that peptides spanning the bilayer are not structured strictly in the α canonical helix structure. When the biological processes involve helix–helix associations or conformational changes as often suggested in signal transduction, helix alterations could play a major role.

References

[1] W.T. van Gunsteren, H.J.C. Berendsen, Angew. Chem. Int. Ed. Engl. 29 (1990) 992.
[2] P. Duan, P. Wilkosz, M. Crowley, J.M. Rosenberg, J. Mol. Biol. 272 (1997) 553.
[3] F. Gaudin, D. Genest, G. Lancelot, Eur. Biophys. J. 26 (1997) 239.
[4] M. Philippopoulos, A.M. Mandel, A.G. Palmer III, C. Lim, Proteins 28 (1997) 481.
[5] W.T. van Gunsteren, F.J. Luque, D. Timms, A.E. Torda, Annu. Rev. Biophys. Biomol. Struct. 23 (1994) 847.
[6] J. Walshaw, J.M. Goodfellow, J. Mol. Biol. 231 (1993) 392.
[7] N. Thanki, J.M. Thornton, J.M. Goodfellow, J. Mol. Biol. 202 (1988) 637.
[8] J. Tirado-Rives, W.L. Jorgensen, Biochemistry 30 (1991) 3864.
[9] K.A. Dill, Biochemistry 29 (1990) 7133.
[10] K.A. Dill, S. Bromberg, K. Yue, et al., Protein Sci. 4 (1995) 561.
[11] M. Levitt, B.H. Park, Structure 1 (1993) 223.
[12] A. Wallqvist, D.G. Covell, Biophys. J. 71 (1996) 600.
[13] F. Fraternali, W.T. van Gunsteren, J. Mol. Biol. 256 (1996) 939.
[14] B.A. Wallace, M. Cascio, D.L. Mielke, Proc. Natl. Acad. Sci. U.S.A. 83 (1986) 9423.
[15] G. von Heijne, Annu. Rev. Biophys. Biomol. Struct. 23 (1994) 167.
[16] C.S. Wu, A. Hachimori, J.T. Yang, Biochemistry 21 (1982) 4556.
[17] M.S. Briggs, D.G. Cornell, R.A. Dluhy, L.M. Gierasch, Science 233 (1986) 206.
[18] R.C. Keller, J.A. Killian, B. de Kruijff, Biochemistry 31 (1992) 1672.
[19] Z. Wang, J.D. Jones, J. Rizo, L.M. Gierasch, Biochemistry 32 (1993) 13991.
[20] J. Johansson, T. Szyperski, T. Curstedt, K. Wuthrich, Biochemistry 33 (1994) 6015.
[21] P. Doruker, I. Bahar, Biophys. J. 72 (1997) 2445.
[22] L.K. Iyer, S. Vishveshwara, Biopolymers 38 (1996) 401.
[23] I.D. Kerr, H.S. Son, R. Sankararamakrishnan, M.S. Sansom, Biopolymers 39 (1996) 503.
[24] D.J. Tobias, J. Gesell, M.L. Klein, S.J. Opella, J. Mol. Biol. 253 (1995) 391.
[25] M. Watanabe, J. Rosenbusch, T. Schirmer, M. Karplus, Biophys. J. 72 (1997) 2094.
[26] C. Bolterauer, H. Heller, Eur. Biophys. J. 24 (1996) 322.
[27] P. Huang, J.J. Perez, G.H. Loew, J. Biomol. Struct. Dyn. 11 (1994) 927.
[28] K. Merz, B. Roux, Biological Membranes. A Molecular Perspective from Computation and Experiment. Birkhäuser, Boston, 1996, 594.
[29] T. Yamamoto, S. Ikawa, T. Akiyama, et al., Nature 319 (1986) 230.
[30] C.I. Bargmann, M.C. Hung, R.A. Weinberg, Cell 45 (1986) 649.
[31] N.E. Hynes, D.F. Stern, Biochim. Biophys. Acta 1198 (1994) 165.
[32] F.J. Lofts, H.C. Hurst, M.J. Sternberg, W.J. Gullick, Oncogene 8 (1993) 2813.
[33] S.O. Smith, C.S. Smith, B.J. Bormann, Nat. Struct. Biol. 3 (1996) 252.
[34] J.P. Duneau, N. Garnier, M. Genest, J. Biomol. Struct. Dyn. 15 (1997) 555.
[35] J.P. Duneau, D. Genest, M. Genest, J. Biomol. Struct. Dyn. 13 (1996) 753.
[36] I. TRIPOS Associates. 1699 South Hanley Road, Suite 303, St. Louis, Missouri 27.
[37] R.L. Dunbrack, M. Karplus, J. Mol. Biol. 230 (1993) 543.
[38] M. Elder, P. Hitchcock, R. Mason, G.G. Shipley, Proc. R. Soc. Lond. A. 354 (1977) 157.
[39] T.J. McIntosh, S.A. Simon, Biochemistry 25 (1986) 4948.
[40] T.J. McIntosh, S.A. Simon, Annu. Rev. Biophys. Biomol. Struct. 23 (1994) 27.
[41] T.B. Woolf, B. Roux, J. Am. Chem. Soc. 116 (1994) 5916.

[42] A. Brünger, C.L. Brooks III, M. Karplus, Chem. Phys. Lett. 105 (1984) 495.
[43] A.T. Brunger, X-PLOR Manual, Yale University, 1992.
[44] B.R. Brooks, R.E. Bruccoleri, B.D. Olafson, D.J. States, S. Swaminathan, M. Karplus, J. Comp. Chem. 79 (1983) 187.
[45] K.V. Damodaran, J.K.M. Merz, B.P. Gaber, Biochemistry 31 (1992) 7656.
[46] M.J.D. Powell, Math. Program. 12 (1977) 241.
[47] A. Blume, Biochemistry 22 (1983) 5436.
[48] J.P. Ryckaert, G. Ciccotti, B.H.J.C., J. Comput. Phys. 23 (1977) 327.
[49] G. Lipari, A. Szabo, J. Am. Chem. Soc. 104 (1982) 4546.
[50] G. Lipari, A. Szabo, J. Am. Chem. Soc. 104 (1982) 4559.
[51] R.W. Pastor, Curr. Opin. Struct. Biol. 4 (1994) 486.
[52] I.A. Kaltashov, C. Fenselau, Proteins: Struct. Func. Genet. 27 (1997) 165.
[53] Y.Y. Shi, L. Wang, W.F. van Gunsteren, Mol. Simulat. 1 (1988) 369.
[54] T.B. Woolf, B. Roux, Proc. Natl. Acad. Sci. U.S.A. 91 (1994) 11631.
[55] T.B. Woolf, B. Roux, Proteins: Struct. Func. Genet. 24 (1996) 92.
[56] L. Shen, D. Bassolino, T. Stouch, Biophys. J. 73 (1997) 3.
[57] B. Roux, T. Woolf, Biological membranes. A molecular perspective from computation and experiment (1996) 555.
[58] T. Woolf, Biophys. J. 73 (1997) 2376.
[59] K. Belohorcova, J.H. Davis, T.B. Woolf, B. Roux, Biophys. J. 73 (1997) 3039.
[60] W.J. Gullick, A.C. Bottomley, F.J. Lofts, et al., EMBO J. 11 (1992) 43.
[61] C.H. Heldin, Cell 80 (1995) 213.
[62] N. Garnier, D. Genest, J.P. Duneau, M. Genest, Biopolymers 42 (1997) 157.
[63] C.L. Burke, M.A. Lemmon, B.A. Coren, D.M. Engelman, D.F. Stern, Oncogene 14 (1997) 687.
[64] H. Cao, L. Bangalore, B.J. Bormann, D.F. Stern, EMBO J. 11 (1992) 923.
[65] Y. Hu, K. Kostov, A. Perico, S. Smithline, K.F. Freed, J. Chem. Phys. 103 (1995) 9091.